# NMR Structures Reveal How Oxidation Inactivates Thrombomodulin†

Matthew J. Wood,‡ L. Amaya Becvar,‡ Judith Helena Prieto, Giuseppe Melacini, and Elizabeth A. Komives*

*Department of Chemistry and Biochemistry, University of California, San Diego, 9500 Gilman Drive, La Jolla, California 92093-0359*

*Received April 23, 2003; Revised Manuscript Received August 1, 2003*

ABSTRACT: Oxidation of Met 388, one of the three linker residues connecting the fourth and fifth EGF-like domains of thrombomodulin (TM), is deleterious for TM activity. An NMR structure of the smallest active fragment of TM (TMEGF45) and a crystal structure of a larger fragment (TMEGF456) bound to thrombin both show that Met 388 is packed into the fifth domain. Using multidimensional NMR, we have solved the structure of TMEGF45 in which Met 388 is oxidized (TMEGF45ox) and the structure of TMEGF45 in which Met 388 is mutated to Leu (TMEGF45ML). Comparison of the structures shows that the fifth domain has a somewhat different structure depending on the residue at position 388, and several of the thrombin-binding residues are packed into the fifth domain in the oxidized protein while they are exposed and free to interact with thrombin in the native structure and the Met-Leu mutant. This observation is consistent with kinetic measurements showing that the $K_m$ for TMEGF45ox binding to thrombin is 3.3-fold higher than for the native protein. Most importantly, the connection between the two domains, as indicated by interdomain NOEs, appears to be essential for activity. In the TMEGF45ox structure which has a reduced $k_{cat}$ for protein C activation by the thrombin−TMEGF45ox complex, interaction between the two domains is lost. Conversely, a tighter connection is observed between the two domains in TMEGF45ML, which has a higher $k_{cat}$ for protein C activation by the thrombin−TMEGF45ML complex.

The biological activity of many proteins can be significantly affected by oxidation of methionine to methionine sulfoxide. Proteins that show decreased activity upon oxidation include calmodulin (*1*), $\alpha_1$-protease inhibitor (*2*, *3*), high mobility group protein HMG-D (*4*), chymotrypsin (*5*), and thrombomodulin (*6*).

Oxidation of Met 388 in thrombomodulin (TM)[1] with chloramine T or $H_2O_2$ results in a 75−90% loss of cofactor activity (*6*). The physiological function of TM, which is an endothelial cell surface glycoprotein, is to form a 1:1 complex with thrombin. When thrombin is in complex with TM, it no longer has procoagulant fibrinogen cleavage activity, but instead has new anticoagulant function to activate protein C (*7*). This process is essential for maintenance of hemostasis (*8*, *9*). The 81-amino acid TM fragment composed of the fourth and fifth EGF-like domains (TMEGF45) is the smallest active TM fragment (Figure 1) (*10*). Cofactor activity assays and binding kinetic studies have shown that

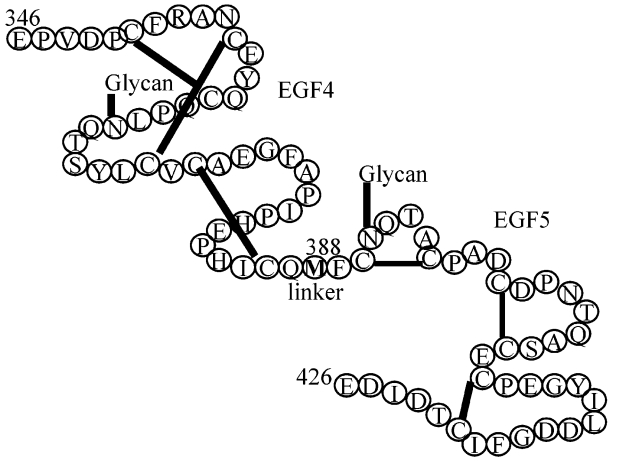


FIGURE 1: Schematic diagram of the smallest active fragment of thrombomodulin. The amino acids are indicated in single letter code and Met 388 is in bold. The disulfide bonding pattern determined previously (*16*) is indicated in solid lines between the cysteine residues. The two N-linked glycosylation sites are indicated with flags.

TMEGF45 has full cofactor activity (as measured by $k_{cat}$ for protein C activation by the thrombin−TMEGF45 complex), but binds to thrombin 10-fold less tightly than the fragment of TM that also contains the sixth domain (Baerga-Ortiz unpublished). Met 388 is located in the short three-residue linker between the fourth and fifth EGF-like domains. It is conserved in mouse, bovine, and human TM, and if Met 388 is mutated to any other residue other than Leu, the cofactor activity of TM decreases (*11*).

† This work was supported by NIH Grants HL47463 and HL70999.

* To whom correspondence should be addressed: Department of Chemistry and Biochemistry, University of California, San Diego, 9500 Gilman Dr., La Jolla, CA 92093-0378. Ph: (858) 534-3058; FAX: (858) 534-6174. E-mail: ekomives@ucsd.edu.

‡ These two authors contributed equally.

[1] Abbreviations: thrombomodulin, TM; epidermal growth factor, EGF; trifluoroacetic acid, TFA; nuclear magnetic resonance, NMR; *N*-acetylglucosamine, GlcNac; TMEGF45, the fragment of thrombomodulin containing the fourth and fifth EGF-like domains; TMEGF45ox, the fragment of thrombomodulin containing the fourth and fifth EGF-like domains and Met388 oxidized; TMEGF45ML, the fragment of thrombomodulin containing the fourth and fifth EGF-like domains but with Met 388 substituted for Leu; heteronuclear nuclear Overhauser effects, hNOEs.

10.1021/bi034646q CCC: $25.00 
Published on Web 09/26/2003

Structural studies of TMEGF45 (*12*) and of the TMEGF-456−thrombin complex (*13*) suggest that Met 388 may play a critical function in the interaction between the fourth and fifth EGF-like domains of TM. In both structures, Met 388 is the central player in side chain interactions that connect the fourth and fifth domains. Alanine mutagenesis revealed that Phe 376, located in the fourth domain, is critical for cofactor activity, and this residue is seen to participate in many hydrophobic contacts with Met 388 (*12*−*14*). In addition, Met 388 is seen inserted into the disulfide bonded core of the fifth domain, interacting mainly with the Cys 390−Cys 395 and Cys 409−Cys 421 disulfide bonds (*12*, *13*). In the structure of the fifth domain alone, Met 388 does not interact with these disulfide bonds and has no apparent structural role (*15*). In comparing the structure of the fifth domain alone with that of the fifth domain in TMEGF45, we hypothesized that insertion of Met 388 into the hydrophobic core of the fifth domain may function to expose the thrombin-binding residues within the fifth domain (*12*). These residues pack against the disulfide bonds in the structure of the fifth domain alone, but are solvent-exposed in the structure of TMEGF45. It is also possible that the interaction between Phe 376 and Met 388 may connect the fourth and fifth domains in a way that perhaps is important for anticoagulant cofactor activity.

Because Met 388 makes extensive hydrophobic contacts with both the fourth and fifth domains, oxidation of this residue could have a large effect on the structure and function of both domains. We present here the structure of TMEGF45 in which Met 388 has been oxidized (TMEGF45ox) and the structure of TMEGF45 in which Met 388 has been mutated to Leu (TMEGF45ML). A comparison of both structures with the wild-type protein reveals that an interdomain connection modulated by the residue at position 388 is critical for thrombin-binding and anticoagulant cofactor activity.

## EXPERIMENTAL PROCEDURES

*Preparation of $^{15}$N-Labeled Proteins.* The TM fragment TMEGF45 corresponds to residues E346-E426 (81 amino acids) with an additional two amino acids (His-Met) on the N-terminus. TMEGF45ML was produced in exactly the same way as TMEGF45 except that residue 388 was mutated to leucine by site-directed mutagenesis using standard protocols. Both TMEGF45 and TMEGF45ML were expressed both unlabeled and uniformly $^{15}$N-labeled in *Pichia pastoris*, purified, and characterized as previously described (*16*, *17*).

*Oxidation of TMEGF45 with $H_2O_2$.* To prepare TMEGF-45ox, TMEGF45 was lyophilized in six 1-mg portions, resuspended to a final concentration of 0.1 mM in oxidation buffer (0.2 M $H_2O_2$, 93 mM sodium phosphate, 0.28 M sodium chloride, 9.3% (w/v) mannitol at pH 7.3), and reacted for 4 h at 23 °C (*6*). The oxidation reaction was quenched by acidification to pH 3.5 with HCl and the samples were immediately injected on a Waters C18 reverse-phase column (19 × 300 mm) equilibrated with 0.1% TFA. TMEGF45ox was eluted with a gradient of 0.1% TFA, 0−20% acetonitrile over 10 min, 20−40% acetonitrile over 40 min at a flow rate of 10 mL/min. Peaks corresponding to TMEGF45ox were lyophilized, assayed for specific activity, and analyzed by mass spectrometry. To verify that the TMEGF45 was completely oxidized, samples were deglycosylated and analyzed on a Perseptive Biosystems Voyager DE STR MALDI-TOF mass spectrometer. To do this, lyophilized TMEGF45 and TMEGF45ox were resuspended in $H_2O$ to ∼0.1 mM, and were mixed 1:10 with matrix. The matrix used for all TM samples consisted of a saturated solution of 10 mg of sinapinic acid (Aldrich Chemicals) suspended in 0.3 mL of acetonitrile and 0.7 mL of 2% TFA. Besides Met 388, the TMEGF45 expressed in *P. pastoris* contains an additional His and Met at the N-terminus, retained from its secretion signal (*10*). MALDI-TOF mass spectrometry of the deglycosylated protein showed that the difference in mass between TMEGF45 and TMEGF45ox was consistent with addition of two oxygen atoms (32 mass units) in TMEGF45ox, one to each of the two methionines.

*Kinetic Measurements.* The kinetics of the reaction of TM with thrombin that result in the production of activated protein C are described by three kinetic constants: $K_m$ for TM binding to thrombin ($K_{mTM}$), $K_m$ for protein C binding to the TM-thrombin complex ($K_{mPC}$), and $k_{cat}$ for the conversion of protein C to activated protein C. The kinetic constants for TMEGF45, TMEGF45ox, and TMEGF45ML were measured as previously described (*10*). The thrombin concentration was 0.1 nM, protein C concentrations were 0.2, 0.4, 1, 2, and 4 $\mu$M, and the chromogenic substrate (S-2366, Chromogenix, Inc.) concentration was 0.015 mg/mL. The TMEGF45ox concentrations used were 0, 200, 500, 1000, 1250, 1500, and 2000 nM at 1 $\mu$M protein C and 0, 200, 500, 1000 nM at all other protein C concentrations. The TMEGF45 and TMEGF45ML concentrations used were 0, 50, 100, 200, 300, 400, and 500 at 1 $\mu$M protein C and 0, 50, 300, 500 nM at all other protein C concentrations. A nonlinear regression of plots of $v$ versus [TM] and $v$ versus [PC] yielded the $K_{mTM}$ and the $K_{mPC}$, and these values were then used to solve the equation for the $V_{max}$. The $K_m$'s were measured at six different TM and five different PC concentrations, and the error was determined as the standard deviation of these measurements.

*NMR Spectroscopy.* All samples used in NMR experiments for the TMEGF45ox and TMEGF45ML structure determinations were prepared from lyophilized protein resuspended in either 90% $H_2O$/10% $D_2O$ or 100% $D_2O$ with 2 mM $NaN_3$ at pH 6.5. $^{15}$N-labeled sample concentrations were between 0.8 and 1.0 mM with a final volume of 0.45 mL, and unlabeled sample concentrations were 1.5 mM with a final volume of 0.5 mL. The pH was adjusted by adding aliquots of 100 mM NaOH or NaOD. Although the oligosaccharides are not essential for TM cofactor activity, they are essential for solubility, and all of the structures solved here were of fully glycosylated protein (approximately 5 kDa in sugars).

All experiments were collected at 310 K on a Bruker DRX600 spectrometer operating at 600.13 MHz. Data collected for the assignments and structure determination included the following 2D experiments: a sensitivity and gradient enhanced ($^1$H,$^{15}$N) HSQC with 512($^1$H) × 256 ($^{15}$N) complex data points (*18*); 2D TOCSY (*19*, *20*) experiments with a 75 ms mixing time in both $H_2O$ and $D_2O$; and 2D NOESY (*21*, *22*) experiments with a 150 ms mixing time in both $H_2O$ and $D_2O$ with 512 scans. Three-dimensional NMR experiments included 50 and 150 ms mixing time $^{15}$N NOESY−HSQC experiments collected with 512($^1$H) × 64-($^{15}$N) × 128($^1$H) complex data points and 48 scans. An HNHA experiment (*23*) was collected to measure $^3J_{HNH\alpha}$

coupling constants. Hydrogen/deuterium exchange experiments collected at 20 min intervals showed all amides were fully exchanged by 2 h. The $\{^1H\}$-$^{15}N$ steady-state NOEs were determined by recording spectra in the presence and absence of a proton presaturation period of 3 s achieved with 120° $^1H$ pulses applied every 5 ms. Each experiment was run in triplicate, collected with 512 × 256 complex points and 48 scans.

*Resonance Assignments, Distance and Dihedral Angle Restraints.* Assignments were done using the Felix Assign module as described for TMEGF45. NOE distance restraints were derived from 3D $^{15}N$-edited NOESY−HSQC and 2D $D_2O$ NOESY spectra. Peak volumes were integrated and converted to interproton distances for each spectrum separately. Distance restraints were classified into three ranges, strong (1.8−3.0 Å), medium (1.8−4.0 Å), and weak (1.8−5.0 Å). Comparison of the TMEGF45, TMEGF45ML, and TMEGF45ox HSQC spectra showed that some cross-peaks had different chemical shifts, while the rest were very similar to those of TMEGF45. Residues that were significantly different were reassigned using the $^{15}N$ NOESY−HSQC spectra. For TMEGF45ox, these included six residues in the fourth domain and 12 residues in the fifth domain. The proline spin systems were assigned using the $D_2O$ TOCSY and NOESY spectra. For TMEGF45ML, these included four residues in the fourth domain and five residues in the fifth domain.

Backbone $\phi$ dihedral angle restraints were derived from $^3J_{HNH\alpha}$ values from the HNHA experiment: $^3J_{HNH\alpha}$ values >8 Hz = −120(±30)° and $^3J_{HNH\alpha}$ values <5 Hz = −90-(±30)°. Rotameric states of $\chi^1$ were estimated from short mixing time TOCSY−HSQC and NOESY−HSQC as previously described (*12, 24*).

*Structure Calculations.* The TMEGF45ox and TMEGF-45ML structures were calculated using the NMR_Refine module of InsightII 98.0 for DGII distance geometry. Structures were minimized using both Discover and XPLOR (*25*) as previously described for TMEGF45 (*12*). The starting structure in all DGII calculations was created by using the lowest energy TMEGF45 structure, which included the core GlcNac sugars, and either oxidizing the residue to the R diastereomer of methionine sulfoxide (for TMEGF45ox) or replacing Met 388 with Leu (for TMEGF45ML) in the Insight 98.0 module *Biopolymer*. The TMEGF45 structures all contain six disulfide bonds and the fifth domain has uncrossed disulfide bonds that form three loops, the N-loop (residues Cys 390−Cys 395) the B-loop (residues Cys 399−Cys 407) and the C-loop (residues Cys 409−Cys 421). The disulfide bonds were included in all structures used in the iterative assignment process as they have been determined chemically (*16*).

For the TMEGF45ox structure, 749 restraints from the $^{15}N$ NOESY−HSQC and $D_2O$ NOESY were initially used to calculate 50 structures using DGII. For the TMEGF45ML structure, 996 restraints were used. In the early rounds of structure calculations, the NOE force constant was set to 1.00 kcal mol$^{-1}$ A$^{-2}$. After this round of calculations, the three structures with the lowest energy and no NOE distance violations were used for further assignments in several iterative rounds that each used three structures as input. Dihedral angles were included at the penultimate round of calculations. The final DGII calculation included 877 NOE distance restraints and 33 dihedral angle restraints. The NOE distance restraints consisted of 390 intraresidue, 250 sequential, 69 medium-range, and 168 long-range restraints. The force constant was set to 30 kcal mol$^{-1}$ A$^{-2}$ for both the distance and dihedral angle restraints. Fifty structures were optimized using simulated annealing for 50 000 steps of 0.2 ps and those with error functions < 3.0 were subjected to 500 steps of conjugate gradients minimization. All resulting minimized structures were then refined using XPLOR (*26*). The same standard slow cooling refinement protocol as was used for TMEGF45 was used to refine the TMEGF45ox and TMEGF45ML structures (*12*). For TMEGF45ox, out of the 39 minimized structures, 23 had no NOE violations > 0.5 Å and no dihedral angle violation > 5°. From these, 12 structures were chosen based on good agreement with experimental data and low energy.

For the TMEGF45ML structure, the final DGII calculation included 1085 NOE distance restraints and 28 dihedral angle restraints. The NOE distance restraints consisted of 497 intraresidue, 291 sequential, 92 medium-range, and 205 long-range restraints. The same DGII protocol and XPLOR refinement as already described for the TMEGF45ox structure was used for the TMEGF45ML structure calculations. Out of 49 minimized structures, 24 had no NOE violations > 0.5 Å and no dihedral angle violation > 5°. From these, 10 structures were chosen based on good agreement with experimental data and low energy. The final structural ensembles for TMEGF45ox and TMEGF45ML were analyzed using Diamond and Procheck NMR as previously described for TMEGF45 (*12*).

*Structural Analysis.* The average domain−domain angle and domain−domain twist (dihedral) for the structural ensembles of TMEGF45, TMEGF45ox, and TMEGF45ML were determined using the *DeCipher* module of Insight 98.0. For each individual molecule in each ensemble, the angle made between a vector drawn from the Cα of residue 388 to the center of mass for the fourth domain (including residues 349−386), and a vector between the Cα of residue 388 and the fifth domain (including residues 390−421) was measured. Also, the dihedral angle made between a vector drawn from the backbone nitrogen of residue 388 and the center of mass for the fourth domain, and a vector drawn from the Cα of residue 388 and the center of mass of the fifth domain was determined.

## RESULTS

*Kinetics of Protein C Activation by TMEGF45ox and TMEGF45ML.* To investigate the differences in biological function between TMEGF45, TMEGF45ox, and TMEGF-45ML, the kinetic parameters of protein C activation by thrombin and TM were measured. TM is an essential activator for the thrombin-mediated activation of protein C, and two Michaelis constants are therefore required, $K_{mTM}$ for the activator and $K_{mPC}$ for the substrate. The $k_{cat}$ for protein C activation by the thrombin−TMEGF45ox complex was also determined (*10*). The values for the kinetic parameters are shown in Table 1 and compared to those for the wild type protein, which were remeasured but agreed well with those previously reported (*10*). The $k_{cat}$ for protein C activation by TMEGF45ox was 3.5-fold lower, 1.4 s$^{-1}$ compared to the wild type $k_{cat}$ of 5.0 s$^{-1}$. The $k_{cat}$ for protein

Table 1: Kinetic Parameters for the Various TMEGF45 Variants

| TM fragment | $K_{m\ TM}$ (nM) | $K_{m\ PC}$ (mM) | $k_{cat}$ ($s^{-1}$) | $k_{cat}/K_{m\ PC}$ ($s^{-1}\ mM^{-1}$) | specific activity (U/mg) |
|---|---|---|---|---|---|
| TMEGF45 | 140 ± 5 | 0.32 ± 0.1 | 5.0 ± 0.1 | 15.6 ± 0.3 | $3.5 \times 10^5$ |
| TMEGF45ML | 140 ± 40 | 0.38 ± 0.1 | 7.8 ± 0.5 | 20.8 ± 7.8 | $5.1 \times 10^5$ |
| TMEGF45ox | 460 ± 70 | 0.42 ± 0.1 | 1.4 ± 0.1 | 3.3 ± 0.4 | $5.0 \times 10^4$ |

C activation by TMEGF45ML was 1.6-fold higher compared to wild type. Although the $K_{mTM}$ for wild type and TMEGF45ML were the same, oxidation of Met 388 increased the $K_{mTM}$ 3.3-fold from 140 to 460 nM. These results agree with previous reports that the $K_d$ of the TM−thrombin interaction increased from 4.4 to 10.9 nM upon oxidation of full-length TM (*11*). These results, on variants of TMEGF45, reinforce our previous assertion that the sixth domain simply adds 10-fold in binding affinity, but does not change the overall structure/function properties of TM (*10*). The results show that oxidation affects TMEGF45 in two ways. It weakens the TM−thrombin interaction and it slows down the catalysis of protein C activation by the TM−thrombin complex. The kinetic parameters expose the dual role of Met 388 in TMEGF45 function and suggest that there are significant structural changes occurring in TMEGF45 upon Met 388 oxidation.

*NMR Resonance Assignments for TMEGF45ox and TMEGF45ML*. The HSQC spectra of TMEGF45ox and TMEGF45ML were very similar to that of TMEGF45, making the assignment process straightforward. The spin system corresponding to residue 388 was identified from sequential connections to Phe 389. Although others have reported that the oxidized methionine may exist as two diastereomers that are interconverted slowly on the NMR time scale, we observed a single spin system for the oxidized Met 388 (data not shown). Residues that showed significant changes in chemical shift upon oxidation of Met 388 included Glu 346, Val 348, Ala 373, Phe 376, Ala 377, and Glu 382 in the fourth domain; Met 388 in the linker; and Cys 395, Ala 394, Ser 406, Glu 408, Gly 412, Tyr 413, Leu 415, Asp 415, Asp 416, Leu 420, Cys 421, and Asp 423 in the fifth domain. Residues that showed significant changes in chemical shift upon mutation of Met 388 to Leu were Val 348, Tyr 358, and Phe 376 in the fourth domain; Leu 388 in the linker; and Cys 390, Ala 394, Cys 395, Cys 407, and Cys 409 in the fifth domain (Figure 2).

*Structure Determination.* For both TMEGF45ox and TMEGF45ML, 50 structures were generated using distance geometry, simulated annealing refinement, and energy minimization, incorporating 877 NOE restraints and 33 dihedral angle restraints for TMEGF45ox (Table 2), and 1085 NOE restraints and 28 dihedral angle restraints for TMEGF45ML (Table 3). Although the 877 NOEs seem substantially less than the 943 NOEs used for the TMEGF45 structure calculation, the predominant difference is in intraresidue restraints, which numbered only 390 for TMEGF45ox compared to 493 for TMEGF45, and in long-range restraints between the linker and the fifth domain, for which TMEGF45ox has none.

For TMEGF45ox, the average overall XPLOR energy was 376 kcal/mol with the NOE and dihedral angle energies contributing just 42.7 and 0.675 kcal/mol, respectively (Table 2A). For TMEGF45ML, the average overall XPLOR energy was 410 kcal/mol with the NOE and dihedral angle energies contributing 42.4 and 1.19 kcal/mol, respectively (Table 2B). These overall energies were comparable to those obtained for the TMEGF45 structure, and all the other XPLOR

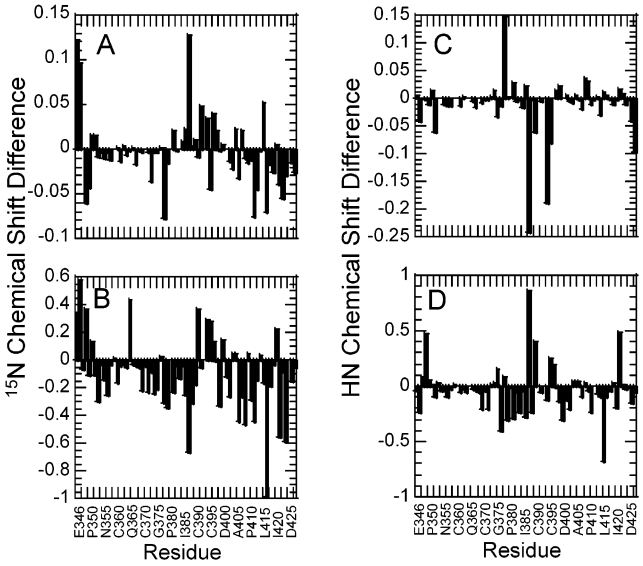


FIGURE 2: Plot of the differences in chemical shift values for the amide protons of TMEGF45ox vs TMEGF45 (A) and of TMEGF45ML vs TMEGF45 (C) and plot of the differences in chemical shift values for the amide nitrogens of TMEGF45ox vs TMEGF45 (B) and of TMEGF45ML vs TMEGF45 (D).

Table 2: Structure Statistics for the Ensemble of 12 Structures of TMEGF45ox

| distance restraints | TMEGF45ox | fourth | fifth | linker |
|---|---|---|---|---|
| intraresidue ($i - j = 0$) | 390 | 243 | 121 | 26 |
| sequential ($\|i - j\| = 1$) | 250 | 160 | 79 | 11 |
| medium-range ($1 < \|i - j\| \leq 1$) | 69 | 53 | 16 | 0 |
| long-range ($\|i - j\| > 4$) | 168 | 134 | 13 | 21 |
| total | 877 | 590 | 229 | 58 |
| NOEs per residue | 10.8 | 14.4 | 6.4 | 19.3 |
| angle restraints | | | | |
| phi dihedral | 33 | 18 | 12 | 3 |
| rmsd (±SD) from experimental restraints[a] | | | | |
| all NOE restraints (Å) | 0.040 ± 0.002 | | | |
| dihedral angles (deg) | 1.17 ± 0.25 | | | |
| rmsd (±SD) from idealized geometry[b] | | | | |
| bond lengths (Å) | 0.011 ± −0.0001 | | | |
| angles (deg) | 2.18 ± 0.093 | | | |
| energies (kcal/mol) | | | | |
| $E_{tot}$ | 376 ± 23 | | | |
| $E_{restraint}$[c] | 42.7 ± 5.1 | | | |
| $E_{dih}$ | 0.675 ± 0.30 | | | |

[a] None of the 12 structures had NOE violations > 0.5 Å or dihedral angle violations > 5°. Rmsd was calculated by finding the mean and standard deviation between the 12 structures. [b] Idealized geometry was defined by the CHARMM force field implemented within XPLOR. [c] The final values of the square-well NOE and dihedral angle potentials were calculated with force constants of 30 kcal $mol^{-1}$ $Å^{-2}$ in DGII and with force constants of 50 kcal $mol^{-1}$ $Å^{-2}$ in XPLOR.

Table 3: Structural Statistics for the Ensemble of 10 Structures of TM45ML

| distance restraints | TMEGF45ML | fourth | fifth | linker |
|---|---|---|---|---|
| intraresidue ($i - j = 0$) | 497 | 306 | 160 | 31 |
| sequential ($\|i - j\| = 1$) | 291 | 196 | 81 | 14 |
| medium-range ($1 < \|i - j\| \leq 1$) | 92 | 66 | 25 | 1 |
| long-range ($\|i - j\| > 4$) | 205 | 144 | 37 | 24 |
| total | 1085 | 712 | 303 | 70 |
| NOEs per residue | 13.4 | 8.8 | 3.7 | 0.9 |
| angle restraints | | | | |
| phi dihedral | 28 | 13 | 14 | 1 |
| rmsd (±SD) from experimental restraints[a] | | | | |
| all NOE restraints (Å) | 0.039 ± 0.002 | | | |
| dihedral angles (deg) | 1.81 ± 0.39 | | | |
| rmsd (±SD) from idealized geometry[b] | | | | |
| bond lengths (Å) | 0.011 ± 0.0001 | | | |
| angles (deg) | 2.27 ± 0.092 | | | |
| energies (kcal/mol) | | | | |
| $E_{tot}$ | 410.0 ± 20.6 | | | |
| $E_{restraint}$[c] | 42.4 ± 3.6 | | | |
| $E_{dih}$ | 1.19 ± 0.33 | | | |

[a] None of the 12 structures had NOE violations > 0.5 Å or dihedral angle violations > 5°. Rmsd was calculated by finding the mean and standard deviation between the twelve structures. [b] Idealized geometry was defined by the CHARMM force field implemented within XPLOR. [c] The final values of the square-well NOE and dihedral angle potentials were calculated with force constants of 30 kcal mol$^{-1}$ Å$^{-2}$ in DGII and with force constants of 50 kcal mol$^{-1}$ Å$^{-2}$ in XPLOR.

Table 4: RMSD of Cartesian Coordinates (Å) for the TMEGF45 Variants

| atoms | backbone | all heavy |
|---|---|---|
| (A) RMSD of Cartesian Coordinates (Å) for TMEGF45ox | | |
| fourth domain (residues 349−364, 368−389) | 1.11 | 1.58 |
| fifth domain (residues 387−390, 394−399, 407−421) | 2.56 | 3.22 |
| TMEGF45ox (residues 349−364, 368−389, 387−390, 394−399, 407−421) | 4.50 | 5.00 |
| (B) RMSD of Cartesian Coordinates (Å) for TMEGF45ML | | |
| fourth domain (residues 349−364, 368−389) | 1.16 | 1.58 |
| fifth domain (residues 387−390, 394−399, 407−421) | 2.12 | 2.69 |
| TMEGF45ML (residues 349−364, 368−389, 387−390, 394−399, 407−421) | 2.16 | 2.54 |

parameters were very similar to those for TMEGF45. None of the final structures had NOE violations > 0.5 Å or dihedral angle violations > 5°. Analysis of the $\phi$ and $\psi$ angles of the 10 structures using PROCHECK_NMR shows that 90% of the (nonglycine and proline) residues fall within the allowed regions of the Ramachandran plot.

*Structural Variation of the Fourth Domain.* Structures of TMEGF45 and the TMEGF456−thrombin complex both show Met 388 playing at least two structural roles. First, the side chain of Met 388 is an integral part of hydrophobic packing of the fifth domain, and oxidation of it to methionine sulfoxide could cause disruption of these hydrophobic interactions. Second, Met 388 is also the main mediator of the fourth and fifth domain−domain interaction; therefore, disrupting it could cause major changes in the orientation of the two domains.

The structure of the fourth domain in TMEGF45ox is very similar to structures of the fourth domain solved previously (Figure 3) (*17*, *27*). The root-mean-squared deviation (rmsd) of the fourth domain overlaid on these residues is 1.11 Å for the backbone atoms and 1.58 Å for all the heavy atoms (Table 4A). These rmsd values are very similar to 1.19 and 1.68 Å values for TMEGF45. For TMEGF45ML, the rmsd of the fourth domain overlaid on residues 349−364 and 368−389 is also similar to TMEGF45: 1.16 Å for the backbone atoms and 1.58 Å for all the heavy atoms (Table 4B).

Figure 3 shows the final structural ensembles of the NMR solution structures of each TMEGF45 variant that has been solved overlaid on the fourth domains. For both TMEGF45ox and TMEGF45ML, the fourth domain forms a $\beta$-sheet between residues Tyr 358 and Cys 372 as confirmed by interstrand NOEs and by the $^3J_{HNH\alpha}$ values > 8.0 Hz for Tyr 358, Gln 361, Thr 366, Leu 369, Val 371, and Cys 372. In TMEGF45ox, the loop of the $\beta$-turn that is glycosylated at Asn 364 appears to be more restrained than it was in the fourth domain of TMEGF45. This is a result of more long-range NOEs assigned for Tyr 368 to residues Pro 350, Cys 351, Ala 354, and Asn 355 in the N-terminus and a new NOE restraint between Thr 366 and Pro 350. These new restraints serve to pack the $\beta$-turn and sheet tightly against the N-terminus.

For TMEGF45ML, most of the fourth domain resembles the overall fold of the wild-type structure. The fourth domain still forms a $\beta$-sheet between residues Tyr 358 and Cys 372 as confirmed by interstrand NOEs and by the $^3J_{HNH\alpha}$ values > 8.0 Hz for Tyr 358, Cys 360, Gln 361, Leu 369, and Cys 372. However, the structures notably diverge at the C-loop of the fourth domain containing Phe 376, a region very well-determined for all structures. Many more long-range NOEs were observed to Phe 376 in the $D_2O$ NOESY spectrum for TMEGF45ML (38) than in TMEGF45 (21) and TMEGF45ox (23). One prominent difference is that long-range NOEs were observed between Phe 376 and Tyr 358, which were not observed in the spectra for TMEGF45 or TMEGF45ox. Also, more strong NOEs were observed from Leu 388 to Phe 376. The additional restraints structure the C-loop differently than in TMEGF45 and TMEGF45ox, with a bend in the backbone toward the fifth domain.

*Structural Variation of the Fifth Domain.* Similar to the TMEGF45 structure, few long-range NOEs, which are critical for any NMR structure determination, were observed in the fifth domain of TMEGF45ox. There were 13 long-range restraints in the fifth domain in TMEGF45ox, compared to 22 in the structure of TMEGF45. The fewer long range restraints did not result in a significantly less resolved fifth domain, because in TMEGF45 many of the long-range restraints did not serve to resolve the structure of the fifth domain, as they were from Met 388 to the Cys 390−Cys 395 and Cys 409−Cys 421 disulfide bonds. In the TMEGF-45ox NOESY spectra these peaks were not observed, resulting in eight less long-range restraints. Long-range NOE restraints observed in the fifth domain of TMEGF45ox that were not present in the TMEGF45 data were between Ala 405 and Phe 419, Ala 394 and Asp 425, Ala 394 and Cys 421, Cys 399 and Cys 407, Cys 409 and Cys 421, and Leu 415 and Cys 421. The new restraints between Ala 405 and Phe 419 and between Leu 415 and Cys 421 draw the thrombin-binding residues Tyr 413-Asp 417 back into the

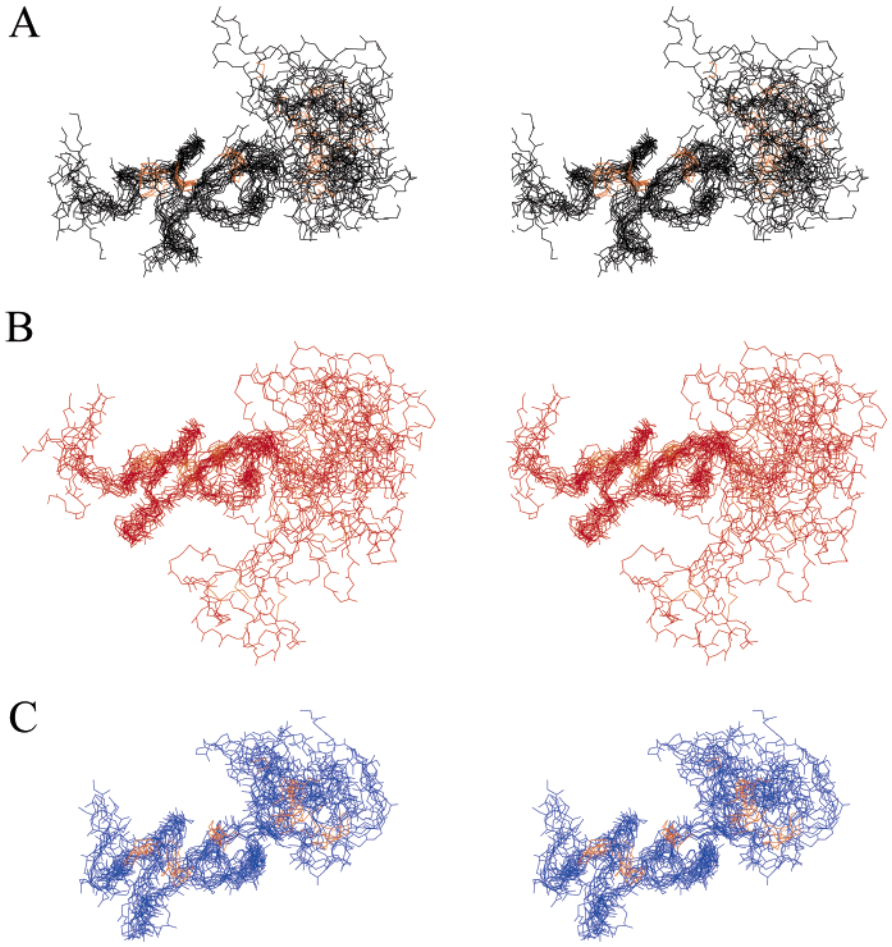


FIGURE 3: Stereoviews of the overlay of the backbone atoms of TMEGF45 (A), TMEGF45ox (B), and TMEGF45ML (C). The molecules are superimposed on the fourth domain residues. The backbone atoms are all displayed in black and the disulfide bonds are displayed in orange. The structures were all superimposed and then displayed separately to ensure a consistent orientation. The N-terminus is on the left and the C-terminus is on the right in each structure. The fifth domain of TMEGF45 is defined to a specific quadrant of space by the long-range NOEs from Met 388 to the fifth domain. The fifth domain of TMEGF45ML is also defined to a narrow quadrant, but it is rotationally distinct from the wild-type structure. The TMEGF45ox structure lacks interdomain NOEs and therefore the orientation of the fifth domain is not defined with respect to the fourth domain.

domain so that they are not as free to interact with thrombin. These new NOEs result in a structure of the fifth domain in TMEGF45ox that is remarkably different from the fifth domain in TMEGF45 (Figure 4). Consistent with the assignment of just 13 long-range NOEs, the rmsd of the backbone atoms was 2.56 Å, a slightly higher value than the 2.33 Å for the fifth domain from TMEGF45 (Table 4A).

Likewise, compared to that for the fourth domain, few long-range NOEs were observed in the fifth domain of TMEGF45ML, though the number of long-range NOEs in the fifth domain TMEGF45ML (*34*) was slightly higher than for TMEGF45. These additional NOEs lead to a somewhat better resolved fifth domain, with an rmsd of 2.12 Å (Table 4B). The fifth domain in all three variants of TMEGF45 can be superimposed on the A-loop (residues 390−395), the B-loop (residues 399−407), and the C-loop (residues 409−421) (Figure 4). The C-loop in TMEGF45ML does not pack back against the rest of the domain as it does in the wild type and TMEGF45ox structures, possibly because the side chain of Leu 388 is not long enough to interact with this region of the fifth domain as it did in the wild type. The fifth domain of TMEGF45ox differs from wild type and TMEGF45ML in that the thrombin-binding residues Tyr 413, Ile 414, and Leu 415 have NOEs back to the hydrophobic core of the fifth domain. This was also seen in the structure of the fifth domain alone. The packing of the thrombin binding residues back into the domain seems to correlate with weaker thrombin-binding affinity (20-fold for the fifth domain alone and 4-fold for TMEGF45ox).

*Structural Variation of the Linker between the Fourth and Fifth Domains.* Each structure differed substantially in the linker due to the alterations at Met 388. The linker residues in TMEGF45ox have many long-range NOEs to the fourth domain, particularly to Phe 376. Once oxidized, Met 388 no longer showed long-range NOEs to residues in the fifth domain. The NOEs between the GlcNAc sugar attached to Asn 391 and residues Phe 389 and Ala 377 were also not observed in the TMEGF45ox structure. Therefore, none of the interdomain NOEs between the fourth and fifth domain seen in TMEGF45 were observed in TMEGF45ox. This caused a lack of definition of the position of the fifth domain with respect to the fourth domain (Figure 3).

The linker region of TMEGF45ML had similar numbers of long-range restraints to both the fourth and fifth domains, as were observed for TMEGF45. However, the identity of the interacting residues differed. Long-range NOEs in TMEGF45ML not observed in TMEGF45 occurred between Leu 388 and Ala 397, Gln 387 and Cys 407, and Gln 387

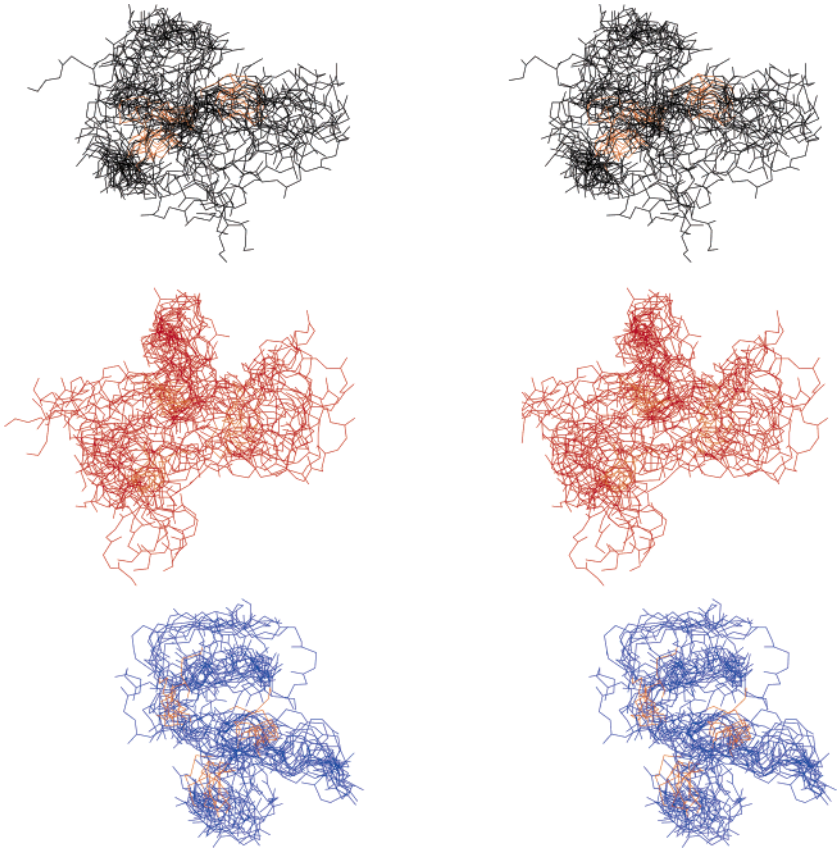

FIGURE 4: Stereoviews of the overlay of the backbone atoms of the fifth domain (residues Gln 387−Asp 426) from TMEGF45 (black), TMEGF45ox (red), and TMEGF45ML (blue). The disulfide bonds in all structures are displayed in orange. The structures were all superimposed and then displayed separately to ensure a consistent orientation. The A-loop is at the bottom left, the B-loop is on the right, and the C-loop is at the top of each set of structures. The positions of the N- and C-termini vary in each set of structures.

and Ser 406. Although Leu 388 had NOEs to the disulfide bonds of the fifth domain as indicated by NOEs to Cys 395, Cys 399, and Cys 407, Leu 388 did not have any NOEs to Cys 421, as were observed in TMEGF45. Presumably the branched side chain of Leu 388 cannot reach as far into the core of the fifth domain. The cysteine spin systems having NOEs to Leu 388 were shifted upfield in comparison to TMEGF45, suggesting that a more hydrophobic environment is provided by the hydrocarbon side chain of Leu 388. Finally, the NOEs between the GlcNAc sugar attached to Asn 391 and residue Phe 389 were subtly different. For TMEGF45, NOEs were observed for the backbone amide proton of Phe 389 to the GlcNAc sugar of Asn 391, which were not seen in TMEGF45ML. Instead, NOEs were observed between the H$\delta$ and H$\epsilon$ protons of Phe 389 and the GlcNAc sugar of Asn 391, NOEs that were not present in TMEGF45.

*Domain−Domain Interactions in TM.* Modular proteins consist of a set of domains that are repeated throughout a continuous amino acid sequence and the NMR and X-ray crystal structures of many multiple domain modular proteins have been solved (*28*−*30*). In some cases, the interdomain linkage has been shown to be fixed, with defined interactions between the two domains (*31*−*34*). While in others, the linkage between the two domains may be completely or at least somewhat ill-defined (*35*−*38*).

The interdomain linkage in TM is hydrophobic, and the residue that mediates the domain−domain interaction is Met 388. The hydrophobicity of Met 388 is apparently critical for the interdomain interactions because in TMEGF45ox, no long-range NOEs are observed between Met 388 and residues in the fifth domain, and this effectively disrupts the fourth and fifth domain−domain interaction. The two domains do not interact with each other, and the linker residues are now exclusively associated with the fourth domain. This causes the domain−domain orientation in TMEGF45ox to be undefined, in contrast to the structure of TMEGF45 (*12*). Consistent with the lack of NOE constraints between the linker and the fifth domain, heteronuclear NOE values for residues in the fifth domain of TMEGF45ox are slightly lower than in the wild-type molecule (Table 5). It is interesting that the heteronuclear NOEs (hNOEs) confirm the differences in side chain interactions (as determined by differences in observed proton−proton NOEs). For example, the oxidized Met 388 retained interactions with Phe376, and the hNOEs for this residue are the same across the variants. The fact that the Leu388 primarily interacts with the C390−

Table 5: Selected Heteronuclear NOE Data for TMEGF45 Variants[a]

| residue | wtTMEGF45 | TMEGF45ox | TMEGF45ML |
|---|---|---|---|
| Phe376 | 0.58 ± 0.02 | 0.60 ± 0.01 | 0.64 ± 0.003 |
| Cys386 | 0.60 ± 0.02 | 0.64 ± 0.02 | 0.58 ± 0.004 |
| Met/Leu388 | 0.55 ± 0.02 | 0.66 ± 0.002 | 0.57 ± 0.06 |
| Phe389 | 0.47 ± 0.06 | 0.42 ± 0.01 | 0.47 ± 0.005 |
| Asn391 | 0.43 ± 0.07 | 0.38 ± 0.02 | 0.39 ± 0.02 |
| Thr393 | 0.39 ± 0.02 | 0.34 ± 0.04 | 0.44 ± 0.08 |
| Cys395 | 0.50 ± 0.03 | 0.48 ± 0.01 | 0.81 ± 0.12 |

[a] Heteronuclear NOE data are presented for a few residues to illustrate the consistency with the presence or absence of proton−proton NOEs. The analysis of all of the relaxation data is complex and will be the subject of a future publication.

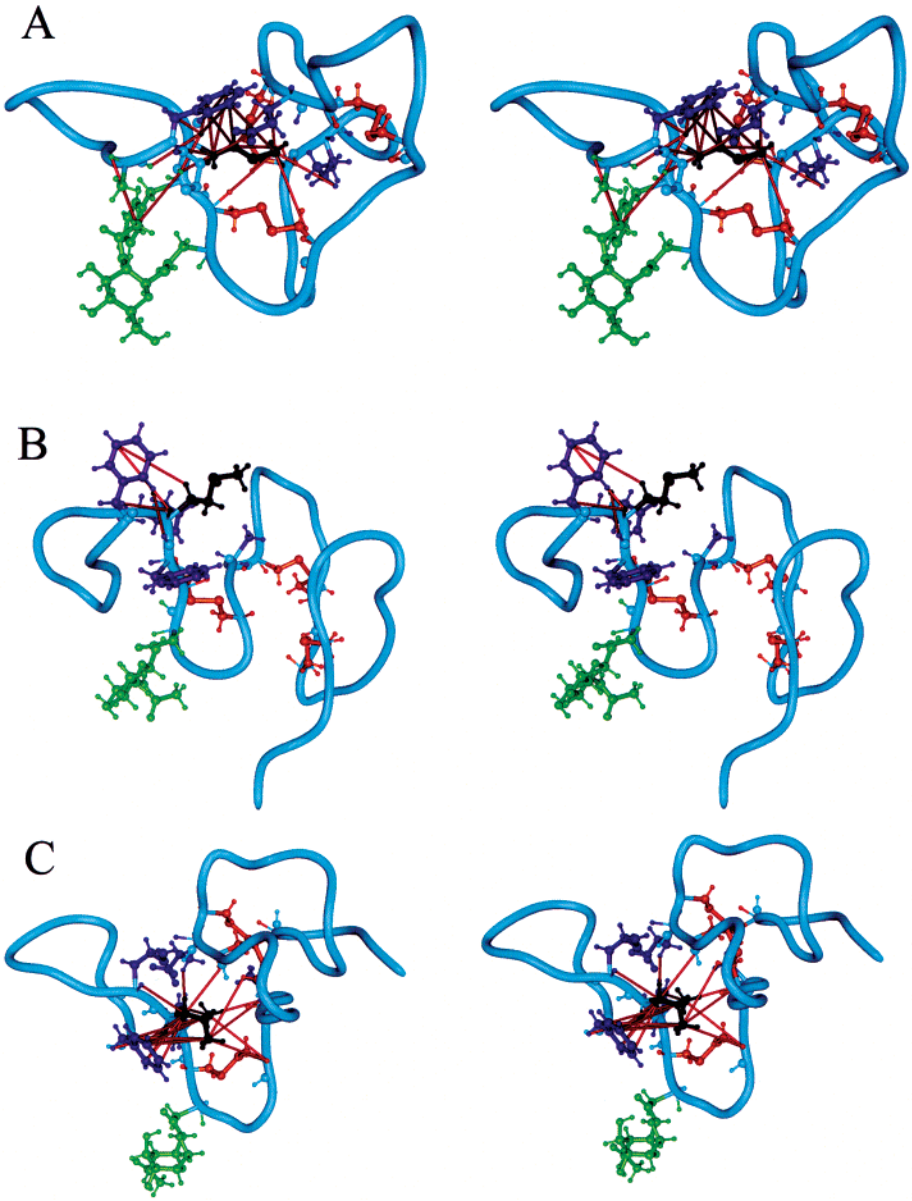


FIGURE 5: Stereoviews of the TMEGF45 variants from residues 372−426. This part of the structure contains the C-loop of the fourth domain and the entire fifth domain. Side chains are shown in ball-and-stick for the cysteines (colored orange), the residue at position 388 (colored black), and other residues that participate in long-range restraints to the residue at position 388 (colored blue). The restraints are shown as red lines, and the backbone is in cyan. The first GlnNac on Asn 391 in the A-loop of the fifth domain is also shown (colored green). (A) Wild-type TMEGF45, (B) TMEGF45ox, (C) TMEGF45ML.

C395 disulfide bond is reflected in slightly higher hNOEs for C395, and lower hNOEs for C399 compared to wild type. The hNOEs for the A-loop of the fifth domain and the observable cysteines are also lower for the TMEGF45ox as compared to the wild-type protein. A full analysis of the relaxation behavior of the variants requires analysis of data from each individual EGF domain, and will be presented elsewhere.

Figure 3 shows the comparison of the structures of TMEGF45, TMEGF45ox, and TMEGF45ML overlaid on just the fourth domain and linker residues. A comparison was made of the rmsd for the backbone atoms of the entire molecule compared vs that for the fifth domain. For TMEGF45, these values were similar, 2.81 and 2.33 Å, respectively. In contrast, the rmsd for the same backbone atoms in TMEGF45ox is 4.50 Å, which is significantly larger than the rmsd of the fifth domain, 2.56 Å. In TMEGF45, the fifth domain, while not absolutely fixed, is defined to one specific quadrant of space. The average interdomain angle of TMEGF45 was 152 ± 5°, while that for TMEGF45ox was 119 ± 26°. The large standard deviation in the TMEGF45ox structural ensemble is evidence of the wide variability of relative positions of the fifth domain with respect to the fourth.

To ascertain whether the communication between the two domains was important for activity, we also solved the structure of another linker variant, TMEGF45ML. In this structure, as in that for the wild-type protein, the position of the fourth domain relative to the fifth appears to be well-determined, with many long-range restraints spanning from the fifth domain to the fourth mediated through Leu 388 (Figure 5). The relatively fixed orientation in this variant is confirmed by the identity between the rmsd values for the entire molecule (2.16 Å) and for the fifth domain (2.12 Å).

Table 6: Domain−Domain Angle and Twist (dihedral) of TMEGF45 Fragments Made between the Center of Mass of the Fourth Domain and the Center of Mass of the Fifth Domain, as Measured Relative to Residue 388

| | (degrees) | |
|---|---|---|
| TMEGF45 variant | angle between fourth domain and fifth domain[a] | twist (dihedral) between fourth domain and fifth domain[b] |
| TMEGF45 | 152 ± 5 | 133 ± 10 |
| TMEGF45ox | 118 ± 26 | −120 ± 23 |
| TMEGF45ML | 167 ± 3 | 170 ± 9 |

[a] For each individual molecule in each ensemble, the angle made between a vector drawn from the Cα of residue 388 to the center of mass for the fourth domain (residues 349−386), and a vector between the Cα of residue 388 and the fifth domain (residues 390−421) was measured. [b] For each individual molecule in each ensemble, the dihedral angle made between a vector drawn from the backbone nitrogen of residue 388 and center of mass for the fourth domain, and a vector drawn from the Cα of residue 388 and the center of mass of the fifth domain was determined.

Interestingly, although the two domains are tightly oriented with respect to each other, the orientation is not the same as it was in the wild type protein. Table 6 compares the domain−domain angle and twist (dihedral) of TMEGF45 and TMEGF45ML. In TMEGF45ML, the two domains are positioned relative to one another at a significantly wider angle, 167 ± 3°, than for TMEGF45, at 152 ± 5°. An even more marked difference is observed in the twist (dihedral) angle measurement between the fourth and fifth domains: TMEGF45ML has an almost 37° greater twist between the fourth and fifth domains. This difference could in large part be due to the different, tighter interaction seen between Leu 388 and Phe 376 in the TMEGF45ML mutant that results in a different twist angle between the central $\beta$-sheet of the fourth domain and the C-loop.

## DISCUSSION

*The Changing Structures of the TM EGF Domains.* EGF domains are small (approximately 40 residues) domains that contain three disulfide bonds and very little regular secondary structure. At the center of the domain is a $\beta$-sheet. In each of the structures of fourth domains of TMEGF45 variants, the juxtaposition of the central $\beta$-sheet to the C-terminal disulfide bonded loop varies. Thus, it appears that these two structural components can take on subtly different twists depending on side chain interactions that extend long distances. Therefore, mutations in the linker can have an impact on the structure of the fourth domain (Figures 3 and 5).

The fifth domain of TM has an uncrossed disulfide bonding pattern and no regular secondary structure (*15*). Its three-loop structure differs significantly depending on interactions with the linker and the fourth domain. The structure of the fifth domain alone had Met 388 disordered and extensive hydrophobic interactions between residues from the A-loop disulfide and the C-loop disulfide (Cys 390-Cys 395 and Cys 409-Cys 421) with hydrophobic packing from Pro 396, Ala 397, Pro 410, Tyr 413, Ile 414, Leu 415, Phe 419, Ile 420, and Thr 422. In contrast, the fifth domain in TMEGF45 had Met 388 inserted into the hydrophobic core replacing other more hydrophobic residues (*12*). Specifically, the residues Tyr 413, Ile 414, and Leu 415 no longer had NOEs to the disulfide bonds, and the side chains appeared to be completely solvent accessible. Since Ile 414 and Leu 415 are two residues that are critical for interacting with thrombin, a hypothesis was advanced that this structural variation might explain the 20-fold increased binding affinity for TMEGF45 as compared to TMEGF5.

Oxidation of Met 388 apparently decreases the hydrophobicity of the side chain enough that it no longer interacts with the core of the fifth domain (Figure 5). As a result, the fifth domain is now structured differently than it was in TMEGF45. Figure 6 shows a matrix representation of the long-range NOEs seen in the TMEGF45, TMEGF45ox, and TMEGF45ML structures. This matrix summarizes the many differences in long-range NOEs within the fifth domain observed for the various structures. One difference is that in the TMEGF45ox structure, Phe 419 has NOEs from its aromatic ring protons to the methyl group on Ala 405 located in the B-loop of the fifth domain. In the TMEGF45 structure, Phe 419 showed interactions with Pro 396 and Ala 397, but in TMEGF45ox these interactions are not observed. This new interaction between Phe 419 and the B-loop causes a different orientation of the B-loop and fixes the B- and C-loops with respect to each other. Another difference is that the majority of the interactions between the A-loop and the C-loop are not observed in TMEGF45ox (Figure 5). In TMEGF45, Met 388 was critical in bringing the A-loop and C-loop together. The lack of contacts between Met 388 and the Cys 390−Cys 395 and Cys 409−Cys 421 disulfide bonds in the fifth domain of TMEGF45ox apparently causes these loops to be further apart.

The structure of the fifth domain in TMEGF45ML is different still from the other variants (Figure 5). The observed long-range NOEs are also very different from TMEGF45 (Figure 6). Leu 388 has long-range NOEs to the Cys 390−Cys 395 and C399−C407 disulfide bonds, but not with the Cys 409−Cys 421 disulfide bond as was observed for the unbranched side chain of M388 in TMEGF45. As a result, the C-loop does not appear to be as tightly held in TMEGF45ML. In fact, the different interactions of the branched side chain of Leu 388 with the fifth domain appear to be orienting the domain overall at a different angle and twist in relation to the fourth domain.

*Consequences of Oxidation on Thrombin Binding.* One of the functional consequences of Met 388 oxidation is that the TM−thrombin protein−protein interaction is weakened. In the structure of the TMEGF456−thrombin complex, only the fifth and sixth domains contact thrombin, and Met 388 inserts into the fifth domain. It might therefore be concluded that the insertion of Met 388 is essential for maintaining the thrombin-binding capability of the fifth domain (*13*). We previously postulated that the expulsion of the thrombin binding residues Tyr 413, Ile 414, and Leu 415 from the hydrophobic core by the insertion of Met 388 may lead to an improved binding affinity for thrombin as compared to the fifth domain alone. This hypothesis is supported by observations presented here. TMEGF45ox, which has the key thrombin-binding residues packed into the hydrophobic core of the fifth domain, has a weakened $K_{mTM}$ relative to that of TMEGF45. On the other hand, TMEGF45ML, which has an adequately large and hydrophobic residue located in the linker region, and the key thrombin-binding residues exposed for binding, has a $K_{mTM}$ comparable to that of wild type. It

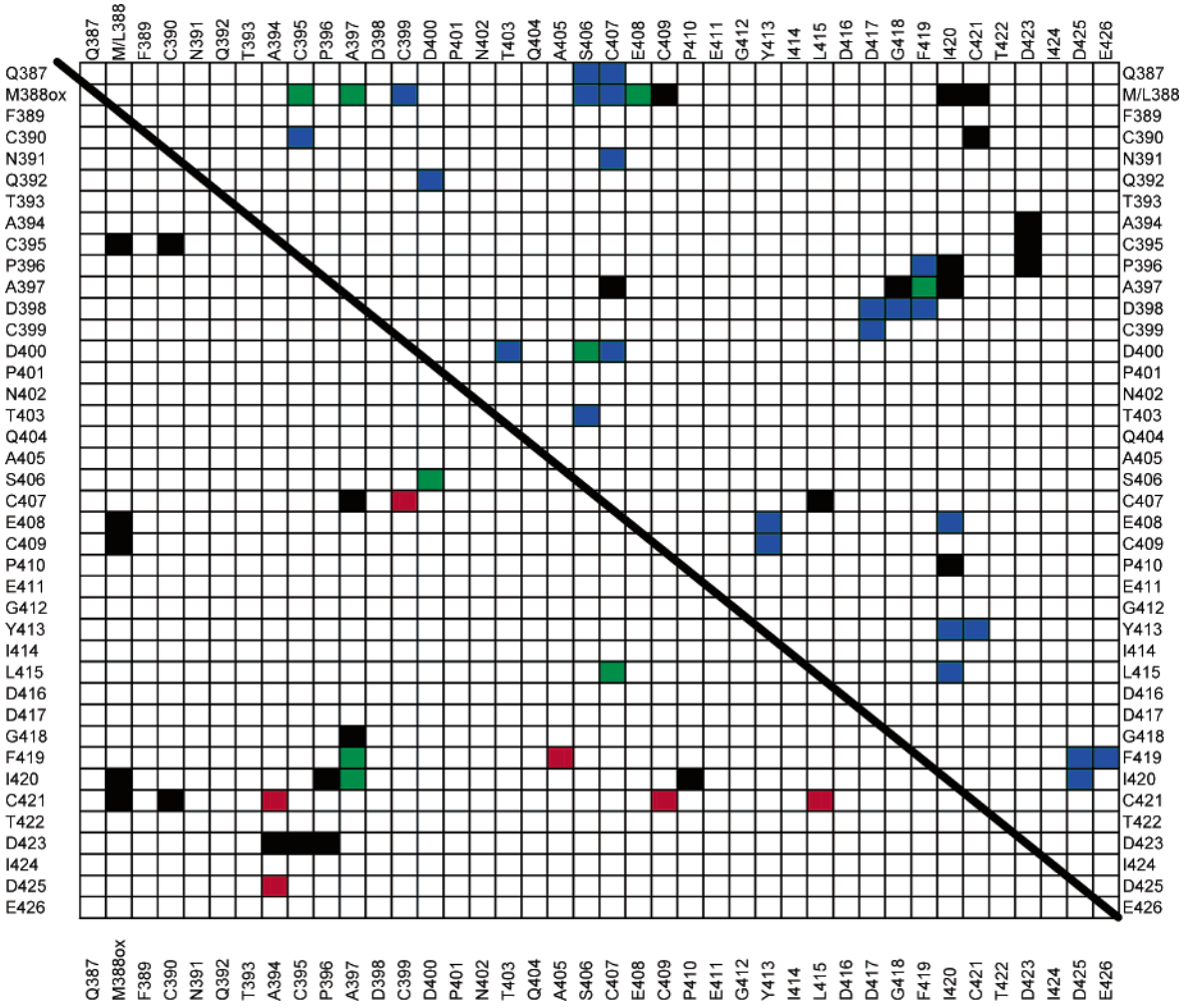


FIGURE 6: Matrix illustration of the long-range restraints in the fifth domain of TMEGF45ox (lower left), and of TMEGF45ML (upper right) compared to wild type. The restraints that are unique to wild-type TMEGF45 as compared to each variant are colored black. The restraints that are unique to TMEGF45ox are colored red. The restraints that are unique to TMEGF45ML are colored blue and the restraints that were observed in both wild type and the variant are shown in green. Side chain assignments for I414 and I424 were ambiguous, and therefore no data were available for these residues.

is interesting to note, however, that the structure of the fifth domain in TMEGF45ML differs from that of TMEGF45 in several ways already described, and yet the thrombin-binding affinity of each of these proteins is equivalent. Thus, the fifth domain appears to be malleable, and most likely binds to thrombin by an induced fit mechanism as we previously proposed (*12*).

*The Importance of Interdomain Communication in TM.* The domain−domain orientation in TMEGF45ox is disrupted, leading to a wider distribution in the structural ensemble that satisfies the restraint set. A similar situation is observed in the NMR structures of the Gla-EGF fragment from coagulation Factor X. The interdomain orientation of this dual domain fragment is stabilized by a $Ca^{2+}$ atom that bridges the two domains, playing the same role that Met 388 does for TMEGF45 (*39*). In the absence of $Ca^{2+}$, the domains are very mobile relative to each other (*40*), which is analogous to what occurs upon Met 388 oxidation in TMEGF45ox.

The lack of definition in the TMEGF45ox interdomain linkage most likely accounts for the 5-fold decrease in the $k_{cat}$ of protein C activation by the TMEGF45ox−thrombin complex. We can make this statement with relative certainty because TMEGF45ML, which has a slightly better than wild type $k_{cat}$, also shows a tight interdomain linkage. Although we can confirm that an interdomain connection is essential for $k_{cat}$, the reason for this still eludes us. Many residues in the fourth domain of TM are essential for protein C activation, but not required for thrombin binding (*14*). The X-ray crystal structure of the TMEGF456−thrombin complex shows that these essential residues do not contact thrombin, and the NMR and X-ray structures show that they are located on a face of TM that most likely contacts protein C (*12*, *13*). One hypothesis is that TM orients protein C for efficient cleavage by thrombin. The fixed, but subtly different, interdomain orientation observed in TMEGF45ML could argue against this hypothesis. On the other hand, the different orientation may more optimally position protein C in the active site of thrombin, leading to the nearly 2-fold improved $k_{cat}$ that is observed for the TMEGF45ML mutant. These speculations await the solution of the ternary complex between thrombin, TM, and protein C.

Methionine oxidation has been shown to affect biological activity, cause conformational changes, and alter the macromolecular interactions of a wide variety of proteins. Amazingly, the addition of one oxygen atom can have a large effect on proteins. In mouse, bovine, and human TM, Met 388 is conserved, but if it is mutated to leucine, the protein

is oxidatively resistant and the cofactor activity increases (*11*). One reason that a methionine is conserved in this position and not the more kinetically optimal leucine may be that the methionine could play a physiological role in rapidly downregulating the anticoagulant potential of TM. Indeed, Met 388 can be efficiently oxidized by activated neutrophils, and neutrophils are known to synthesize inactive TM (*6*, *41*). The functional consequences of the need to maintain oxidative sensitivity of Met 388 may lie, therefore, in the need to maintain a procoagulant environment during inflammation response.

## ACKNOWLEDGMENT

We thank Frank Church and Tim Mather for helpful discussions. M.J.W. was supported by the Heme and Blood Proteins Training Grant from the NIH, A.B. was supported by a GANN fellowship, and J.H.P. was supported by a fellowship from the American Heart Association.

## REFERENCES

1. Gao, J., Yin, D., Yao, Y., Williams, T. D., and Squier, T. C. (1998) *Biochemistry 37*, 9536−48.
2. Johnson, D., and Travis, J. (1979) *J. Biol. Chem. 254*, 4022−6.
3. Carp, H., Miller, F., Hoidal, J. R., and Janoff, A. (1982) *Proc. Natl. Acad. Sci. U.S.A. 79*, 2041−5.
4. Dow, L. K., Changela, A., Hefner, H. E., and Churchill, M. E. A. (1997) *FEBS Lett. 414*, 514−20.
5. Weiner, H., Batt, C. W., and Koshland, D. E., Jr. (1966) *J. Biol. Chem. 241*, 2687−93.
6. Glaser, C. B., Morser, J., Clarke, J. H., Blasko, E., McLean, K., Kuhn, I., Chang, R.-J., Lin, J.-H., Vilander, L., Andrews, W. H., and Light, D. R. (1992) *J. Clin. Invest. 90*, 2565−73.
7. Esmon, C. T. (2000) *Biochim. Biophys. Acta 1477*, 349−60.
8. Griffin, J. H., Ecatt, B., Zimmerman, T. S., Kleiss, A. J., and Widerman, C. (1981) *J. Clin. Invest. 68*, 1370−3.
9. Healy, A. M., Rayburn, H. B., Rosenberg, R. D., and Weiler, H. (1995) *Proc. Natl. Acad. Sci. U.S.A. 92*, 850−4.
10. White, C. E., Hunter, M. J., Meininger, D. P., White, L. R., and Komives, E. A. (1995) *Protein Eng. 8*, 1177−87.
11. Clarke, J. H., Light, D. R., Blasko, E., Parkinson, J. F., Nagashima, M., McLean, K., Vilander, L., Andrews, W. H., Morser, J., and Glaser, C. B. (1993) *J. Biol. Chem. 268*, 6309−15.
12. Wood, M. J., Sampoli-Benitez, B. A., and Komives, E. A. (2000) *Nat. Struct. Biol. 7*, 200−4.
13. Fuentes-Prior, P., Iwanaga, Y., Huber, R., Pagila, R., Rumennik, G., Seto, M., Morser, J., Light, D. R., and Bode, W. (2000) *Nature 404*, 518−25.
14. Nagashima, M., Lundh, E., Leonard, J. C., Morser, J., and Parkinson, J. F. (1993) *J. Biol. Chem. 268*, 2888−92.
15. Sampoli Benitez, B. A., Hunter, M. J., Meininger, D. P., and Komives, E. A. (1997) *J. Mol. Biol. 273*, 913−26.
16. White, C. E., Hunter, M. J., Meininger, D. P., Garrod, S., and Komives, E. A. (1996) *Proc. Natl. Acad. Sci. U.S.A. 93*, 10177−82.
17. Wood, M. J., and Komives, E. A. (1999) *J. Biomol. NMR 13*, 149−59.
18. Palmer, A. G., III., Cavanagh, J., Wright, P. E., and Rance, M. (1991) *J. Magn. Res. 93*, 151−70.
19. Bax, A., and Davis, D. G. (1985) *J. Magn. Res. 65*, 355−60.
20. Braunschweiler, L., and Ernst, R. R. (1983) *J. Magn. Res. 53*, 521−8.
21. Kumar, A., Ernst, R. R., and Wüthrich, K. (1980) *Biochem. Biophys. Res. Commun. 95*, 1−6.
22. Macura, S., and Ernst, R. R. (1980) *Mol. Phys. 41*, 95−117.
23. Vuister, G. W., and Bax, A. (1993) *J. Am. Chem. Soc. 115*, 7772−7.
24. Nooren, I. M. A., Rietveld, A. W. M., Melacini, G., Sauer, R. T., Kaptein, R., and Boelens, R. (1999) *Biochemistry 38*, 6035−42.
25. Brünger, A. T. (1988) *X-PLOR Version 3.1 A System for X-ray Crystallography and NMR*, Yale University Press, New Haven.
26. Nilges, M., Kuszewski, J., and Brunger, A. T. (1991) *Computational Aspects of the Study of Biological Macromolecules by NMR*, Plenum Press, New York.
27. Lougheed, J. C., Bowman, C. L., Meininger, D. P., and Komives, E. A. (1995) *Protein Sci. 4*, 773−780.
28. Campbell, I. D., and Bork, P. (1993) *Curr. Opin. Struct. Biol. 3*, 385−392.
29. Doolittle, R. F. (1995) *Annu. Rev. Biochem.* 287−314.
30. Campbell, I. D., and Downing, A. K. (1998) *Nat. Struct. Biol. NMR Supplement*, 496−499.
31. Brandstettler, H., Bauer, M., Huber, R., Lollar, P., and Bode, W. (1995) *Proc. Natl. Acad. Sci. U.S.A. 92*, 9796−9800.
32. Downing, A. K., Knott, V., Werner, J. M., Cardy, C. M., Campbell, I. D., and Handford, P. A. (1996) *Cell 85*, 597−605.
33. Morgan, W. D., Birdsall, B., Frenkiel, T. A., Gradwell, M. G., Burghaus, P. A., Syed, S. E. H., Uthaipibull, C., Holder, A. A., and Feeney, J. (1999) *J. Mol. Biol. 289*, 113−22.
34. Ulmer, T. S., Werner, J. M., and Campbell, I. D. (2002) *Structure (Camb) 10*, 901−11.
35. Copie, V., Tomita, Y., Akiyama, S. K., Aota, S., Yamada, K. M., Venable, R. M., Pastor, R. W., Krueger, S., and Torchia, D. A. (1998) *J. Mol. Biol. 277*, 663−82.
36. Potts, J. R., Bright, J. R., Bolton, D., Pickford, A. R., and Campbell, I. D. (1999) *Biochemistry 38*, 8304−8312.
37. Saha, S., Boyd, J., Werner, J. M., Knott, V., Handford, P. A., Campbell, I. D., and Downing, A. K. (2001) *Structure (Camb) 9*, 451−6.
38. Beglova, N., North, C. L., and Blacklow, S. C. (2001) *Biochemistry 40*, 2808−15.
39. Sunnerhagen, M., Olah, G. A., Stenflo, J., Forsen, S., Drakenberg, T., and Trewhella, J. (1996) *Biochemistry 35*, 11547−59.
40. Sunnerhagen, M., Forsen, S., Hoffren, A. M., Drakenberg, T., Teleman, O., and Stenflo, J. (1995) *Nat. Struct. Biol. 2*, 504−9.
41. Conway, E. M., Nowakowski, B., and Steiner-Mosonyi, M. (1992) *Blood 80*, 1254−63.

BI034646Q